Earthquakes in Switzerland and surrounding regions during 2014

Tobias Diehl[1],*, Nicolas Deichmann[1], John Clinton[1], Philipp Kästli[1], Carlo Cauzzi[1], Toni Kraft[1], Yannik Behr[1], Benjamin Edwards[1,2], Aurélie Guilhem[1,3], Edith Korger[1], Manuel Hobiger[1], Florian Haslinger[1], Donat Fäh[1], Stefan Wiemer[1]

Key Words Seismicity, Focal mechanisms, Seismotectonics, Diemtigen, Mantle earthquake

[1]Swiss Seismological Service, ETH Zürich, Sonneggstrasse 5, CH-8092 Zürich, Switzerland. (http://www.seismo.ethz.ch)
[2]Now at Department of Earth, Ocean and Ecological Sciences, University of Liverpool, Liverpool L69 3GP, UK.
[3]Now at CEA/DAM/DIF, F-91297 Arpajon, France.
*Corresponding Author: tobias.diehl@sed.ethz.ch

Abstract

During 2014, 817 earthquakes and 180 quarry blasts were detected and located in the region under consideration. An additional 160 earthquakes with $M_L \leq 1.0$ were located using supplementary analysis techniques. The number of located earthquakes in 2014 was the largest since the installation of a seismic network in Switzerland in 1975. This unusually large number is mainly due to the occurrence of two vigorous earthquake sequences, and the local reduction of the earthquake detection thresholds of the Swiss seismic network. With a total of 22 earthquakes of $M_L \geq 2.5$, the seismic activity of larger and potentially felt events was close to the average of 23 earthquakes over the previous 39 years. The most noteworthy seismicity was the earthquake sequence near Diemtigen, west of Lake Thun, where more than 270 events were located between April and December. High-precision hypocenter relocation was applied to image the spatio-temporal evolution of this seismicity. The sequence culminated in an M_L 3.2 event in October, which was felt in the region of Lake Thun and Bern. Other cases of earthquakes felt by the public include earthquakes in the region of Biel (M_L 3.2), in Vallorcine (M_L 3.2), and in Stalden (M_L 3.0). Finally, a small but unusually deep earthquake was recorded beneath the Jura Mountains. Focal depth, apparent velocities, as well as waveform characteristics of this earthquake are consistent with a source in the uppermost mantle. This earthquake is the first reliable record of a sub-Moho event ever observed in Switzerland.

Zusammenfassung

Dieser Bericht des Schweizerischen Erdbebendienstes stellt eine Zusammenfassung der im Vorjahr in der Schweiz und Umgebung aufgetretenen Erdbeben dar. Im Jahr 2014 wurden im erwähnten Gebiet 817 Erdbeben sowie 180 Sprengungen erfasst und lokalisiert. Weitere 160 Beben mit Magnituden $M_L \leq 1.0$ wurden mit Hilfe von zusätzlichen Auswertungsmethoden lokalisiert. Die Zahl der in 2014 lokalisierten Erdbeben ist die höchste seit der Installation eines seismischen Messnetzes in der Schweiz im Jahre 1975. Diese außergewöhnlich hohe Zahl erklärt sich vor allem durch das Auftreten zweier äußerst aktiver Erdbebensequenzen und der lokalen Absenkung der Detektionsschwelle für Erdbeben durch die Verbesserung des seismischen Messnetzes der Schweiz. Mit 22 Beben der Magnitude $M_L \geq 2.5$ lag die seismische Aktivität von stärkeren und potentiell spürbaren Ereignissen im Jahr 2014 nahe am Durchschnitt von 23 Beben pro Jahr der vergangenen 39 Jahren. Bemerkenswert war die Erdbebensequenz von Diemtigen, westlich vom Thunersee bei der mehr als 270 Ereignisse zwischen April und Dezember lokalisiert wurden. Hochauflösende Erdbebenlokalisierung wurde verwendet, um die räumliche und zeitliche Entwicklung dieser Erdbebenserie abzubilden. Ein Beben der Magnitude M_L 3.2 bildete den Höhepunkt der Sequenz im Oktober. Dieses wurde in der Region des Thunersees und Bern deutlich verspürt. Weitere Erdbeben, die von der Bevölkerung verspürt wurden, waren unter anderem die Beben in der Region Biel (M_L 3.2), in Vallorcine (M_L 3.2) und in Stalden (M_L 3.0). Darüberhinaus wurde ein schwaches, aber ungewöhnlich tiefes Erdbeben unterhalb des Juras registriert. Sowohl Herdtiefe, Scheingeschwindigkeiten und Charakter der Wellenformen weisen auf einen Erdbebenherd im obersten Mantel hin. Damit ist dieses Ereignis die erste verlässliche Beobachtung eines Erdbebens unterhalb der Moho in der Schweiz.

Resumé

Ce rapport du Service Sismologique Suisse résume l'activité sismique en Suisse et dans ses régions environnantes au cours de l'année 2014. Pendant cette période, 817 tremblements de terre et 180 tirs de carrière ont été détectés et localisés dans la région. 160 séismes additionnels de magnitude $M_L \leq 1.0$ ont été localisés à

l'aide de moyens supplémentaires d'analyse. Le nombre des évènements localisés en 2014 constitue un record depuis 1975, date de l'installation du réseau sismologique en Suisse. Ce grand nombre inhabituel peut être principalement expliqué par l'occurrence de deux séquences sismiques importantes et par la diminution locale des niveaux de détection résultant des améliorations apportées au réseau sismologique suisse. Avec un total de 22 séismes de magnitude $M_L \geq 2.5$, le nombre des évènements les plus forts et potentiellement ressentis est proche de la moyenne annuelle de 23 tremblements de terre enregistrée pendant les 39 dernières années. La sismicité la plus notable est la séquence sismique qui a eu lieu près de Diemtigen, à l'ouest du lac de Thoune, où plus de 270 évènements ont été localisés entre avril et décembre. La relocalisation de grande précision des hypocentres a permis d'imager l'évolution spatio-temporelle de cette sismicité. La séquence est dominée par un séisme de magnitude M_L 3.2 en octobre qui a été ressenti dans la région du lac de Thoune et à Berne. D'autres tremblements de terre ont été ressentis par la population, tels que ceux de la région de Bienne (M_L 3.2), de Vallorcine (M_L 3.2) et de Stalden (M_L 3.0). Enfin, un faible mais inhabituel séisme profond a été enregistré dans le Jura. Sa profondeur focale, les vitesses apparentes enregistrées ainsi que les caractéristiques des formes d'ondes de ce tremblement de terre sont en accord avec une source dans le manteau supérieur. Par conséquence, ce tremblement de terre est le premier enregistrement fiable d'un évènement ayant eu lieu sous le Moho en Suisse.

1. Introduction

Past earthquake activity in Switzerland and surrounding regions has been documented in a series of annual reports since 1879. A detailed overview on the history of past reports and studies covering different aspects of the recent seismicity of Switzerland is given e.g. by Diehl et al. (2014). The present report first summarizes the state of the seismic network and documents changes in its configuration during 2014. Then we give a short overview on the methods used for earthquake analysis. This is followed by a description of the seismic activity and significant earthquakes in 2014. Finally, we discuss the focal-depth distribution, the occurrence of earthquake sequences, and the unusually large number of earthquakes located in 2014.

2. Data acquisition and analysis

2.1 Seismic stations in operation during 2014

As described in former reports (e.g. Diehl et al. 2014), the Swiss Seismological Service (*Schweizerischer Erdbebendienst*, SED) operates two separate nationwide seismic networks, a high-gain seismometer network predominantly consisting of broad-band instruments (Table A-1 in Appendix 1) and a low-gain accelerometer network (Table A-2 in Appendix 1). In addition, the SED operates a number of temporary stations for various projects (Table A-3 in Appendix 1). SED stations with on-line data acquisition that were operational at the end of 2014 are shown in Fig. 1.

Within the Swiss Strong Motion Network (SSMNet) renewal project, 100 free-field, real-time, very broad-band accelerometer stations are being installed over a 10-year timeframe between 2010 and 2019 (Clinton et al. 2011, Michel et al. 2014). In 2014, 9 new accelerometer stations were installed (SARE, SBAK,

SBAM2, SBAS, SBIF2, SBIK, SLUK, SNES2, SSCN). Two new stations (SMFL, STRW), funded by the state of Liechtenstein, were also installed and are operated by the SSMNet.

The station at ACB was upgraded from a 5s-sensor to a broadband sensor. No other significant changes were made to the high-gain network, though the SED began a project to upgrade all stations. Each existing station will be upgraded to include 1) a very-broad-band sensor (if not yet existing); 2) a modern datalogger with significant local storage to improve final data completeness and lessen the impact of communication outages; and 3) a co-located strong motion accelerometer (if not yet existing). Where necessary, sites will also be re-located or improved to reduce site noise and improve earthquake detectability and signal quality. Additionally, 8 new stations (including 2 new borehole sites in the Alpine foreland) will be added to the network in order to achieve homogenous network spacing across the country.

The NAGRA network, which was installed under a contract with the National Cooperative for the Disposal of Radioactive Waste in northeastern Switzerland (Diehl et al. 2014), is expected to be a long-term network operated by the SED. The 10 new stations (7 surface, 3 borehole) are now included in the broad-band network (Table A-2 in Appendix 1). The SED has begun monitoring microseismicity near the two undergound rock physics laboratories in Switzerland on a long-term basis, funded by various consortia that include the Federal Office of Topography (Swisstopo) and the Swiss Competence Center for Energy Research – Supply of Electricity (SCCER-SoE). At the Mont Terri in NW Switzerland, a strong motion and a broad-band station (MTI01 and MTI02) were installed inside the underground laboratory, and a surface strong motion station (MTI03) directly above it. A surface short period sensor, GSF01, was installed near Grimsel Rock Laboratory, which is the site of the existing SDSNet broad-band station GRIMS, near the Grimsel
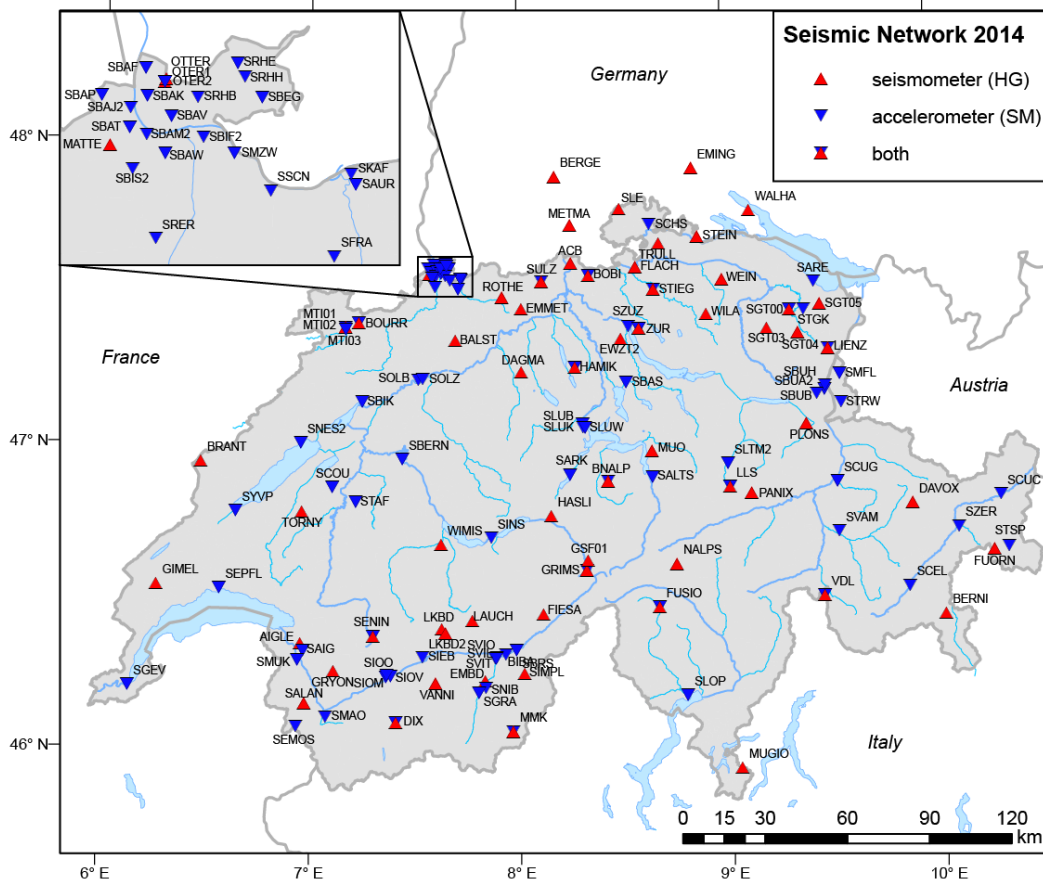
Figure 1 Seismograph stations in Switzerland with on-line data acquisition operational at the end of 2014. The stations defined as high-gain (HG) are mostly equipped with broad-band or 5-second sensors, whereas the strong-motion stations (SM) are accelerometers (see also Table A-1-A-3 in Appendix 1).

Pass. The temporary networks built to monitor geothermal projects in Basel (2006) and Sankt Gallen (2013) continue to operate, albeit with a reduced number of sensors.

Temporary stations are deployed to improve understanding of on-going earthquake sequences in Switzerland. In 2014, a broad-band station continued to operate near Sargans following the M_L 4.1 Balzers (LI) event on December 12th 2013 (Diehl et al. 2014), and a number of stations were installed near Diemtigen (BE), following the vigorous sequence described in this report. In addition to improving the location of local events, the installation of these aftershock stations that have real-time communications also significantly reduces the magnitudes of earthquakes that can be detected.

To improve the reliability of locations for events at the periphery of or outside of Switzerland, the SED continues to be engaged in an on-going cross-frontier cooperative effort to exchange seismic data in real-time with foreign seismic networks as documented in detail by Diehl et al. (2014). With two new stations in Austria and one new station in Italy a total of 44 foreign stations were monitored at the SED in 2014.

2.2 Routine Earthquake Analysis

Methods and software currently used for routine earthquake analysis are described in detail in Diehl et al. (2013, 2014). All events are assigned a local magnitude (M_L) that is calculated from the maximum amplitude of the horizontal components of the seismograms filtered to simulate the response of a Wood-Anderson seismograph (Diehl et al. 2014). In addition, a procedure has been implemented, which routinely and automatically provides estimates of the moment magnitude (M_W) for a subset of events, using a spectral fitting technique (Edwards et al. 2010). Focal mechanisms in 2014 were determined from the azimuthal distribution of first-motion polarities (fault-plane solutions) using the HASH algorithm of Hardebeck and Shearer (2002).

2.3 Supplementary Earthquake Analysis

To lower the detection threshold and to provide robust magnitudes of earthquakes that are too weak to be reliably and consistently detected by the standard automatic detection algorithms of the SED, supplementary analysis methods were applied to selected earthquake sequences in 2014. Template signals (e.g. seismograms of previously detected

earthquakes) were compared to continuous data streams by cross-correlation (CC). Such CC-based algorithms can lower the earthquake detection threshold by one magnitude unit compared to common trigger algorithms like the one implemented in the SeisComP3 monitoring software of the SED (e.g. Schaff and Waldhauser 2010). It should be noted that independent hypocenters cannot be determined for the majority of the events detected by CC, due to the insufficient number of available arrival-time picks. In some cases, however, the number of manually identified P- and S-wave arrivals allows an independent hypocenter location of an event detected by CC. This was the case for 160 events in 2014. The M_L magnitudes of these events are almost exclusively less than 1.0 and, because of the logarithmic nature of the magnitude scale, even attain negative values. A relative magnitude $M_L^{(corr)}$ is assigned to events without independent hypocenter locations using a procedure described in Edwards et al. (2015).

3. **Seismic activity during 2014**

3.1 Overview

During 2014, the Swiss Seismological Service detected and located a total of 817 earthquakes in the region shown in Fig. 2. Based on criteria such as the time of occurrence, the location, and signal character or on direct communication, 180 additional seismic events were identified as quarry blasts. In addition to these events, 160 earthquakes with $M_L \leq 1.0$ have been located by supplementary analysis as described in section 2.3. Magnitude values of the events recorded in 2014 range from M_L -0.4 to 3.3 (Fig. 3). The events with $M_L \geq 2.5$ and the criteria used to assign the quality rating for the given locations as well as the corresponding estimated location uncertainties are listed in Tables 1 and 2. Table 1 also includes the available M_w values derived using the spectral fitting method of Edwards et al. (2010). None of the events in 2014, however, generated sufficient long-period energy to produce a high-quality full-waveform moment-tensor inversion. Fault-plane solutions based on first-motion polarities are shown in Fig. 4 and 5 (see also Fig. 2) and their parameters are listed in Table 3.

Fig. 6 shows the epicentres of the 933 earthquakes with $M_L \geq 2.5$, which have been recorded in Switzerland and surrounding regions over the period 1975 – 2014. These events represent about 7 % of the total number of events detected during that time in the same area. The chosen magnitude threshold of M_L 2.5 ensures that the data set is complete for the given period (Nanjo et al. 2010) and that the number of unidentified quarry blasts and of mislocated earthquakes is negligible.

3.2 Significant earthquakes of 2014

3.2.1 Biel/Bienne (BE)

Two earthquakes of M_L 2.8 and M_L 3.2 occurred within 15 minutes on January 8th about 7 km W of Biel/Bienne (BE) (Fig. 2). Both events were felt by the local population. The stronger of the two reached degree IV on the European Macroseismic Scale EMS-98 (Grünthal 1998). With the closest station BOURR at a distance of 28 km, the focal depth is not well resolved. Including Pg, Sg, and Pn phases in the location procedure results in focal depths of 8 to 10 km for both events. Although uncertainties in focal depths are in the order of ±2-3 km, it is certain that the earthquakes occurred in the crystalline basement beneath the southern edge of the Jura. Focal mechanisms were determined from the analysis of first-motion polarities of both events (Fig. 2 and 4; Table 3). The mechanisms are dominated by normal-fault and strike-slip components with T-axes roughly oriented in NE-SW direction, typical for mid and lower crustal earthquakes in the northern Alpine foreland of Switzerland (e.g. Kastrup et al. 2004, Singer et al. 2014). Uncertainties of the mechanisms are significant (Fig. 4), mainly due to sparse station coverage in the Swiss and French Jura. Nevertheless, the two mechanisms cannot be identical (see for example the change in polarity at station BOURR in Fig. 4), which suggests that either the slip direction on the fault changed between the M_L 2.8 and the M_L 3.2 event or the events occurred on different faults. The two earthquakes triggered a small sequence of 21 locatable earthquakes over the following twelve days with magnitudes ranging between M_L 0.6 and M_L 2.3. Waveforms of these 21 aftershocks show at least two different groups with P-wave signals similar to either the M_L 2.8 or the M_L 3.2 event at station BOURR and CHMF. This observation may support the hypothesis that the M_L 2.8 and the M_L 3.2 events have occurred on different faults.
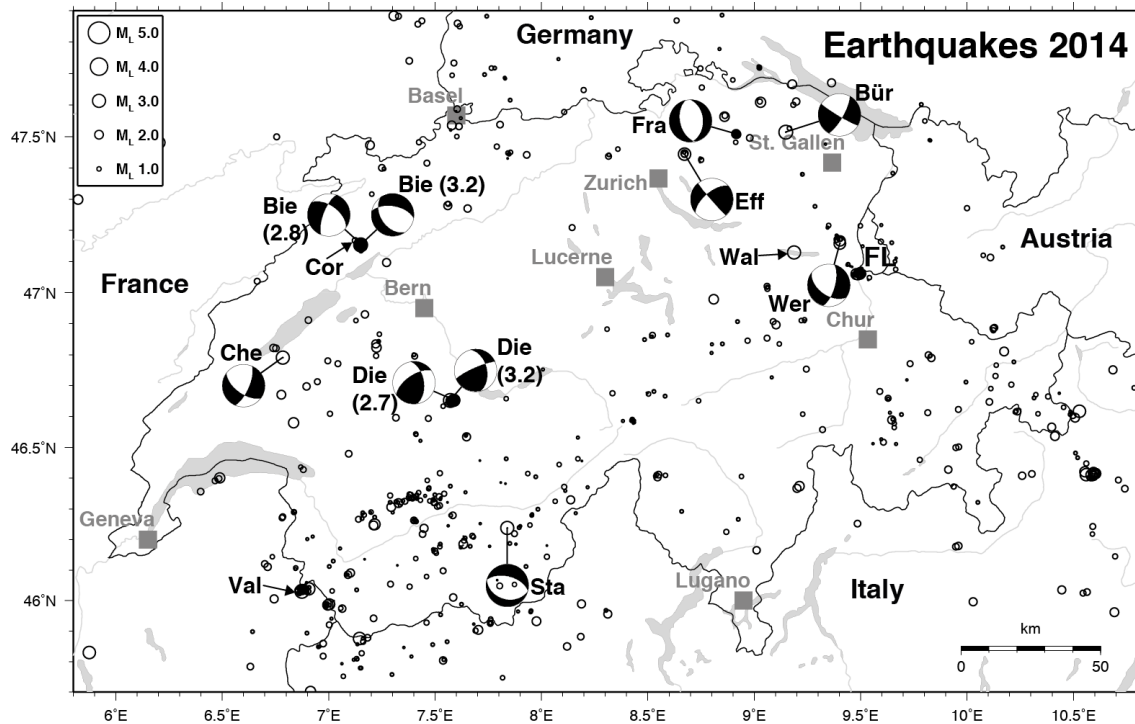
Figure 2 Epicentres and focal mechanisms of earthquakes recorded by the Swiss Seismological Service during 2014. Epicentres of events mentioned in the text are Biel (Bie), Bürglen (Bür), Cheyres (Che), Cortébert (Cor), Diemtigen (Die), Effretikon (Eff), Frauenfeld (Fra), Stalden (Sta), Vallorcine (Val), Walensee (Wal), Werdenberg (Wer). FL marks the territory of Liechtenstein.

3.2.2 Cortébert (BE): the first known event in the upper mantle below northern Switzerland

On January 29th, 2014, 22:37 UTC, a small (M_L 1.4) but unusually deep event occurred 4 km SSE of Cortébert (about 9 km W of Biel below the ridge of the Chasseral; see Fig. 2). Despite the small magnitude of the event and the low signal-to-noise ratio at several stations, reliable first onsets could be picked out to a distance of 120 km (station SLE). The location using all available data (18 P- and 7 S-onsets, including two additional foreign stations) and the 3D velocity model of Husen et al. (2003) gives a focal depth of 38.5 km, with an azimuthal gap of 65 degrees and an RMS of 0.22 s. Other combinations of onsets with distance cut-offs at 50 and 80 km as well as with and without the use of S-arrivals give focal depths between 35.6 km and 36.3 km. The stability of the results with varying data is the first indication for the reliability of the calculated focal depth. Based on the argument that the onsets at larger epicentral distances are generally weaker, and that model errors have a larger effect over longer distances, the location obtained with the available 11 P- and 5 S-onsets out to epicentral distances of 80 km is the preferred location (47.156/7.129, Z= 36 km, GAP = 63° and RMS = 0.07 s). According to Waldhauser et al. (1998) and Wagner et al. (2012), the crust-mantle boundary (Moho) below the epicenter lies at about 28-29 km. Consequently, our location places the hypocenter of this small earthquake clearly in the upper mantle and thus confirms the hypothesis mentioned by Stange et al. (2014). To illustrate this

fact, Fig. 7 shows a seismogram-section along a WSW-ENE trending profile for the Cortébert event, together with a seimogram-section along a W-E trending profile for the M_L 3.2 Courrendlin (JU) event of July 3rd, 2013, 14:13 UTC. According to Diehl et al. (2014), the epicenter of the latter event is about 20 km N and 20 km E of the Cortébert event, with a hypocenter at 25 km in the lower crust. Superimposed on these two record-sections are travel-time curves calculated with a 2D ray-tracing program, that takes into account the Moho topography as determined by Waldhauser et al. (1998), assuming a focal depth of 24 km for the Courrendlin event and of 36 km for the Cortébert event. As one would expect for a lower-crustal event, beyond about 70 km, the first arrival of the Courrendlin event changes from the slower direct wave (Pg) to the faster wave refracted in the upper mantle (Pn). The prominent second arrival visible in the three traces beyond 80 km is the superposition of the Pg and the reflection at the Moho discontinuity (PmP). In the seismograms of the Cortébert event, on the other hand, there is no visible kink in the travel-time curve of the first arrivals in this distance range, and a distinct secondary phase is entirely lacking. As the calculated travel-time curve shows, this is what is expected for a hypocenter below the Moho. Given the remaining uncertainties of the focal depths, the Moho topography and the seismic velocities, the calculated travel-time curves in Fig. 7 are schematic and merely serve to illustrate the categorical differences between the two events. Nevertheless, the low apparent velocity of the Pg/PmP phase seen in the record-

5

section of the Courrendlin event (6.2 km/s) is evidence for the lack of high-velocity material present over any substantial depth interval in the lower crust of northwestern Switzerland. Moreover, the large amplitude of the reflected phase (PmP) requires a sharp velocity discontinuity at the crust-mantle transition.

The Cortébert event is thus the first documented earthquake with a hypocenter in the upper mantle below the northern Alpine foreland of Switzerland. Supplementary analysis of signals at station BOURR (epicentral distance ~27 km) detected 3 additional events in 2014, which all occurred on February 19th (see section 2.3 for details). These events were slightly smaller than the M_L 1.4 event and could not be located. The similarity of waveforms with the M_L 1.4 event, however, indicates that the three detected events were located very close to this event. Though the magnitudes of these four events are small ($M_L \leq 1.4$), it shows that, contrary to previous observations, the upper mantle in this region is not entirely aseismic.
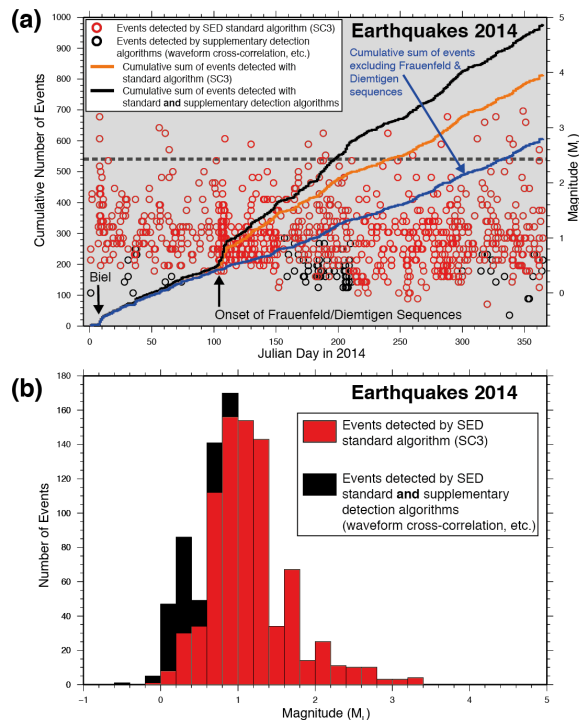

Figure 3 Earthquake activity during 2014: **a** timeline showing magnitude of each event and cumulative number of events (arrows mark the onsets of the Biel, Frauenfeld, and Diemtigen sequences); **b** magnitude histogram. Removing events detected by supplementary algorithms and events associated with the two sequences results in 607 events in 2014 (blue curve in a), which is close to the average number of 541 events/year (horizontal dashed grey) over the last 12 years.

3.2.3 Stalden (VS)

Many people in the Rhône and Visper Valley felt the M_L 3.0 earthquake, which occurred on February 25th (00:52 UTC) close to the village of Stalden (VS).

About 120 felt reports were collected and the maximum observed intensity was IV. The focal depth of 6 ± 1 km is well constrained by several nearby weak- and strong-motion stations and is consistent with a source in the upper Penninic Nappes. The extensional focal mechanism shown in Fig. 4 (see also Fig. 2) is well constrained by first motion polarities of P-phases and is consistent with previous seismicity and the general extensional regime expected south of the Rhône Valley (e.g. Kastrup et al. 2004).

3.2.4 Frauenfeld (TG)

Between April 16th and April 18th a sequence of 38 earthquakes occurred about 5 km S of Frauenfeld (TG). Magnitudes in this sequence range from M_L 0.4 to M_L 2.0 and routinely calculated focal depths of 10 ± 1 km show that the source of these earthquakes is within the crystalline basement beneath the Plateau Molasse. The dense seismic network in NE Switzerland permits the calculation of a focal mechanism for the strongest event of the sequence. The distribution of first-motion polarities suggests an almost N-S striking normal-fault mechanism (Fig. 4, 2). The high similarity of waveforms across the sequence allowed the measurement of differential times by cross-correlation, which were used for relative relocation of the hypocenters applying the double-difference technique of Waldhauser and Ellsworth (2000). The relocated hypocenters, shown in Fig. 8, image a planar structure dipping to the west. The dip of about 45° agrees well with the westward dipping plane of the focal mechanism of the strongest event in the sequence (Fig. 4 and 8) and we conclude that this westward dipping plane was also the active rupture plane of the M_L 2.0 event. The sequence initiated at the up-dip edge of the structure and propagated in down-dip direction (Fig. 8). The M_L 2.0 event, which occurred about 32 hours after the first located event of the sequence, locates at the northern edge of the seismicity, about halfway between the up-dip and down-dip end of the structure. The plane outlined by the seismicity corresponds to a fault in the crystalline basement, which also hosted the M_L 2.0 event.

Supplementary analysis of signals at station WEIN (epicentral distance ~6 km) detected 361 additional earthquakes with magnitudes between $M_L^{(corr)}$ -0.8 and $M_L^{(corr)}$ 1.0 (see section 2.3 for details). They all occurred between April 15, 15:39, and April 18, 05:17, except for one $M_L^{(corr)}$ 0.6 event that occurred about 26 hours before that period. What caused the identified fault to rupture in a sequence of about 400 small earthquakes in less than 62 hours remains to be investigated.

Table 1 Earthquakes with $M_L \geq 2.5$. The values listed under M_{WSPEC} are the moment magnitudes calculated from the spectral fitting method documented in Edwards et al. (2010). The quality rating (Q) is defined in Table 2.

Date and time UTC	Lat. (°N)	Lon. (°E)	X/Y (km)	Z (km)	Mag. (M_L)	Mag. (M_{WSPEC})	Q	Location
2014/01/08 18:12:25	47.156	7.152	578/223	8	2.8	2.6	C	Biel, BE
2014/01/08 18:27:49	47.154	7.150	578/222	10	3.2	2.9	C	Biel, BE
2014/02/25 00:52:45	46.239	7.839	625/86	6	3.0	2.8	A	Stalden, VS
2014/03/02 13:19:12	45.830	5.875	478/76	7	2.9	---	C	Savoie, F
2014/03/05 08:55:50	47.061	9.480	755/214	7	2.6	2.5	A	Balzers, FL
2014/04/19 10:35:04	45.877	7.145	577/80	2	2.8	2.7	B	Col du Gd. St-Bernard, VS
2014/05/10 01:43:48	46.654	7.588	611/167	9	2.7	2.7	A	Diemtigen, BE
2014/06/25 09:33:55	46.653	7.588	611/167	9	2.7	2.7	A	Diemtigen, BE
2014/07/07 06:46:35	46.412	10.560	840/145	11	2.9	3.0	B	M. Cevedale, I
2014/07/09 01:58:00	46.250	7.215	583/122	7	2.5	2.7	A	Haut de Cry, VS
2014/08/28 11:30:41	46.618	10.527	836/167	11	2.9	2.8	A	Stelvio, I
2014/09/17 15:12:40	46.411	10.583	842/145	12	2.5	2.6	B	M. Cevedale, I
2014/10/10 02:46:32	47.481	6.203	507/259	13	2.7	2.5	C	Montbozon, F
2014/10/15 19:36:33	46.653	7.571	610/167	10	3.2	3.0	A	Diemtigen, BE
2014/11/08 16:04:22	47.445	8.672	693/256	12	2.8	2.6	A	Effretikon, ZH
2014/11/14 04:14:12	47.130	9.186	732/221	0	3.1	3.3	B	Walensee, SG
2014/11/23 20:52:16	46.031	6.873	556/98	5	3.2	3.1	A	Vallorcine, F
2014/12/04 09:29:36	46.039	6.905	559/99	4	2.8	2.7	A	Vallorcine, F
2014/12/07 08:26:37	47.159	9.401	749/225	4	2.7	2.6	A	Werdenberg, SG
2014/12/15 06:58:18	47.514	9.147	729/264	25	3.3	2.8	A	Bürglen, TG
2014/12/17 23:04:27	46.791	6.783	550/182	29	3.1	2.9	A	Cheyres, FR
2014/12/28 06:01:21	45.989	7.002	566/93	7	2.6	2.3	B	Aiguilles du Tour, VS

Table 2 Criteria and location uncertainty corresponding to the quality rating (Q) of the hypocentral parameters in the event list in Table 1. GAP = largest angle between epicentre and two adjacent stations; DM = minimum epicentral distance; H = horizontal location; Z = focal depth.

Rating	Criteria		Uncertainty	
Q	GAP (degrees)	DM (km)	H (km)	Z (km)
A	≤180	≤1.5 x Z	≤2	≤3
B	≤200	≤25	≤5	≤10
C	≤270	≤60	≤10	>10
D	>270	>60	>10	>10

Table 3 Focal mechanism parameters based on first-motion polarities of 10 earthquakes in 2014 (see Figs. 2 and 4 and 5).

Location	Date and time UTC	Depth (km)	Mag.	Plane 1 Strike/Dip/Rake	Plane 2 Strike/Dip/Rake	P-Axis Azimuth/Plunge	T-Axis Azimuth/Plunge
Biel	2014/01/08 18:12:25	8	2.8	306/55/-155	201/70/-38	159/41	257/9
Biel	2014/01/08 18:27:49	10	3.2	280/56/-120	146/44/-53	135/65	31/6
Stalden	2014/02/25 00:52:45	6	3.0	106/35/-89	285/55/-91	192/80	15/10
Frauenfeld	2014/04/17 23:59:24	12	2.0	358/41/-82	167/49/-97	31/83	262/4
Diemtigen	2014/05/10 01:43:48	9	2.7	235/62/134	351/51/37	295/7	197/51
Diemtigen	2014/10/15 19:36:33	10	3.2	246/80/135	346/46/14	303/22	195/38
Effretikon	2014/11/08 16:04:22	12	2.8	139/87/153	231/63/3	188/16	91/21
Werdenberg	2014/12/07 08:26:37	4	2.7	126/51/-149	15/66/-43	334/47	74/9
Bürglen	2014/12/15 06:58:18	25	3.3	121/84/-165	29/75/-6	346/15	254/6
Cheyres	2014/12/17 23:04:27	29	3.1	126/60 /-156	23/69/-32	342/37	76/6

3.2.5 Diemtigen (BE)

A remarkable sequence of earthquakes commenced on April 13 close to the village of Diemtigen (BE), W of the Lake Thun (Fig. 2). By the end of 2014, 274 events with magnitudes between M_L -0.1 and M_L 3.2 were located, and seismic activity continues into 2015. In 2014, the sequence can be divided into three major periods of increased activity: the main pulses in April to May; mid-June to mid-July; and another phase in October. The three largest events occurred on May 10th (M_L 2.7), June 25th (M_L 2.7), and October 15th (M_L 3.2). Regional residents felt all three events, with the strongest event reaching degree IV on the European Macroseismic Scale EMS-98 (Fig. 9).
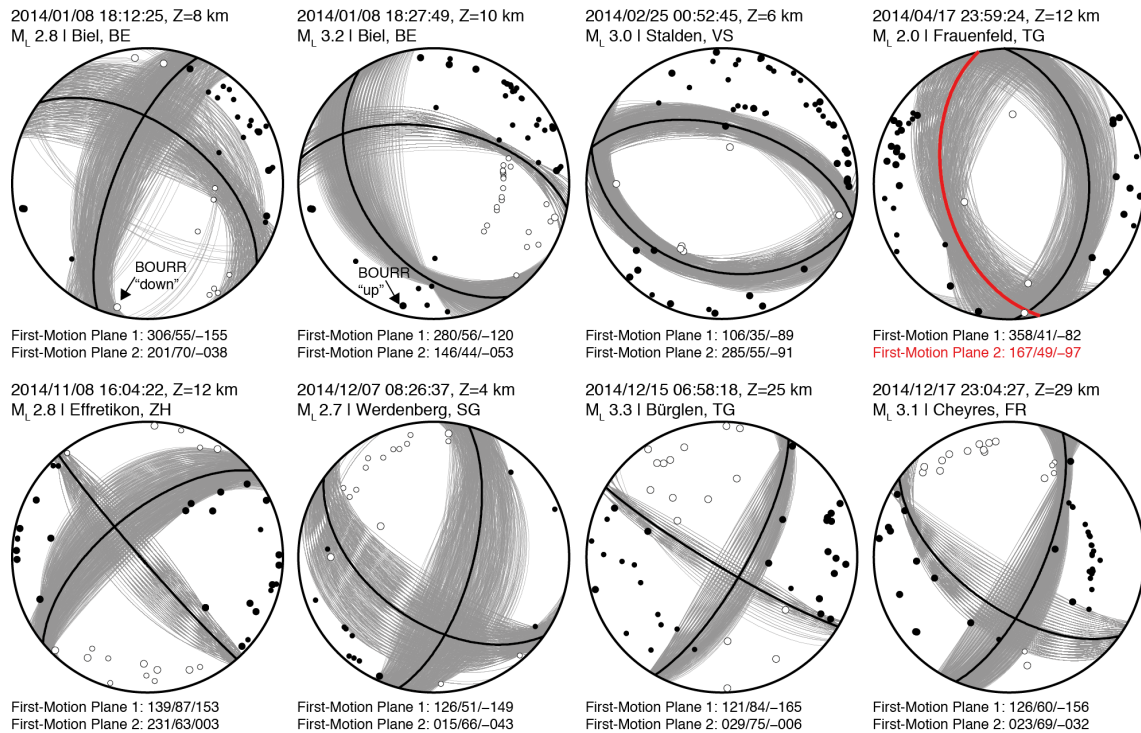
Figure 4 Fault-plane solutions based on first-motion polarities for eight events in 2014 (Biel M_L 2.8 and 3.2, Stalden, Frauenfeld, Effretikon, Werdenberg, Bürglen, Cheyres; see Table 3). All stereograms are lower hemisphere, equal-area projections. Solid circles correspond to compressive first motion (up); empty circles correspond to dilatational first motion (down). The take-off angles were computed with the NonLinLoc software (Lomax et al. 2000), using the 3D velocity model of Husen et al. (2003). Grey lines show sets of acceptable solutions derived by the HASH algorithm (Hardebeck and Shearer 2002); black bold lines indicate the (preferred) average focal mechanisms of all accepted solutions; red bold lines mark the active plane as determined from high-precision relative earthquake relocations.

We used the M_L 3.2 earthquake to compare felt intensities derived from the analysis of macroseismic web questionnaires with instrumental intensities converted from instrumental records of ground motions (ShakeMap; Wald et al. 1999; Worden et al. 2010). The SED ShakeMap shown in Fig. 9 is produced using the state-of-the-art in engineering seismology in Switzerland (ground-motion predictive models, site effect estimates, etc.) as described in Cauzzi et al. (2014). In the case of the M_L 3.2 Diemtigen event, the felt reports suggest higher intensity levels than the instrumental ShakeMap close to the epicenter and in the urban areas of Bern and Interlaken. A good agreement between the ShakeMap and the felt reports is apparent in the town of Thun, on the western shores of Lake Thun, and in the Aare valley, with macroseismic intensities approaching or reaching degree IV. Elevated intensities in the lower Kander valley and the Interlaken region are consistent with areas of higher site amplification, only partly captured by the resolution of the ShakeMap, which is targeted to the national scale. The peak-ground-velocity (*PGV*) of about 0.04 cms^{-1} recorded by the accelerometric station SBERN in Bern corresponds to average intensity levels approaching degree II at most. Note however that the calibration dataset of Faenza and Michelini (2010), used in the SED ShakeMap, shows a large variability of *PGV* values for intensity IV, spanning two orders of magnitude from 0.01 to 1 cms^{-1}. With only one recording

SDSNet station (WIMIS) within 20 km of the epicenter, the Diemtigen event demonstrates that the automatic inclusion of high-quality felt reports into SED ShakeMaps would produce a more complete and possibly better constrained shaking scenario.

To improve the quality of hypocenter locations and to lower the detection threshold of earthquakes associated with the sequence, 3 additional temporary seismic stations were installed at changing locations in the region between June 2014 and April 2015 (for locations see Fig. 10a). All stations were equipped with short-period seismometers and real-time communication. Focal mechanisms could be determined for the May 10th (M_L 2.7) and October 15th (M_L 3.2) events (Fig. 5, 10b). Compared to the event in May, the additional stations in the source region helped to reduce the uncertainties in the mechanisms of the M_L 3.2 event. Both mechanisms correspond to a combination of thrust and strike-slip components (Fig. 5, 10b) with P-axis oriented NE-SW, which is the typical stress-regime observed along the northern front of the Alps and Helvetic domains NE of Diemtigen (Kastrup et al. 2004).

To image the active rupture plane and the spatio-temporal evolution of this unusual sequence, we performed a relative relocation of hypocenters similar to the procedure described for the Frauenfeld sequence. We applied waveform cross-correlation and selected 187 events for the double-difference

relocation shown in Fig. 10b. After relocation, the epicenters cluster much more tightly and cover an area of about 0.7 x 0.4 km (Fig. 10b). Fig. 11a and 11b show two vertical cross-sections that cut two nodal planes of the focal mechanisms, shown in Fig. 5 and 10b. Cross-section AA' (Fig. 11a) suggests that the earthquakes occur on a structure dipping towards ENE, consistent with plane number two (see Fig. 5, 10b) of the focal mechanisms. The seismicity in the vicinity of the October 15th M_L 3.2 event forms a particularly sharp, distinctively dipping structure, which is offset with respect to the May 10th and June 25th events (Fig. 11a). The fine-scale structure of the relocated seismicity in Fig. 11a indicates that the seismicity associated with the sequence is not located on one simple planar structure. Instead, a kink or a bend along the structure seems to separate the structures hosting the events in May and July from the M_L 3.2 event in October (Fig. 11a). Seismicity below the May 10th event appears more diffuse and seems to form an almost horizontal structure at its down-dip end (Fig. 11a).
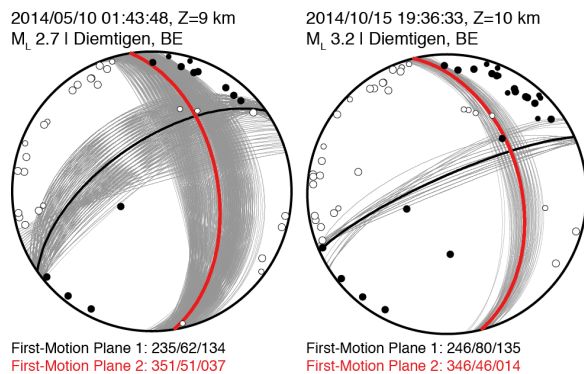
2014/05/10 01:43:48, Z=9 km
M_L 2.7 | Diemtigen, BE

2014/10/15 19:36:33, Z=10 km
M_L 3.2 | Diemtigen, BE

First-Motion Plane 1: 235/62/134
First-Motion Plane 2: 351/51/037

First-Motion Plane 1: 246/80/135
First-Motion Plane 2: 346/46/014

Figure 5 Fault-plane solutions based on first-motion polarities for two events in 2014 (Diemtigen M_L 2.7 May 2014; Diemtigen M_L 3.2 October 2014; see Table 3). Symbols and explanation as in Fig. 5.

Supplementary analysis of signals at station WIMIS (epicentral distance ~4 km) detected 1720 additional earthquakes with magnitudes between $M_L^{(corr)}$ -1.5 and $M_L^{(corr)}$ 0.8 in 2014 (see section 2.3 for details). Results of this analysis indicate, that the Diemtigen sequence already started on March 19, 13:01 (UTC), with an earthquake of magnitude $M_L^{(corr)}$ -0.1, which was too small to be located. Seven template events had to be used to find all previously located events of the sequence. All detected events were associated with one of these templates by means of waveform similarity and therefore belong to one of seven waveforms clusters. Comparing the result of the template-matching analysis to the double-difference relocation shown in Fig. 11, we found that the template events are located in different parts of the imaged structure. The spatial volumes covered by the individual clusters hardly overlap, which allows to estimate the location of all detected events – down to magnitude $M_L^{(corr)}$ -1.5 – to a precision of a few hundred meters by comparing waveforms at a single station.

The relocated seismicity shown in Fig. 11 reveals clear along-dip migration patterns during the evolution of the sequence. As shown in Fig. 11c seismicity initiated at about 8.1 km depth on April 13th and migrated down-dip in the following weeks. The M_L 2.7 event on May 10th occurred around the initial depth of 8.1 km and seismicity following May 10th migrated in up-dip direction. Seismicity in November occurred then on the up-dip periphery of the sequence and the entire sequence covered a depth interval of 0.6 km. Vertical errors in Fig. 11 are relative errors and it should be noted that the accuracy of the absolute depth of the sequence is less well constrained. The accuracy of the absolute source depth is mainly controlled by the quality of the velocity model used for location. Even focal depths determined with 3D regional models can have errors of few kilometers due to the imperfect knowledge of the local velocity structure (e.g. Husen et al. 2012).

The top of the autochthonous crystalline basement in the region of Diemtigen is expected to lie at a depth of about 6-7 km (e.g. Pfiffner et al. 1997a). SW of Diemtigen, geological profiles suggest sediments reach down to 8 km depth below the Niesen nappe (e.g. Pfiffner et al. 1997b). Because of the uncertainties in the absolute focal depth and in the geological interpretation of the seismic data (including along-strike deviation from the 2D profiles) it is not possible to determine whether the sequence occurred in the crystalline basement or in the lowermost part of the overlying sediments. The apparent kinks or bends in the seismogenic structure suggest that the structure might be intersected by sub-horizontal lithological boundaries, which would be indicative for a source in sedimentary units (e.g. Mesozoic sediments).

The Diemtigen sequence shows the typical characteristics of an earthquake swarm, e.g. lack of a distinct main shock, unusually large spatial extent compared to the moment release of the largest individual event, and magnitudes that fail to decay with time (e.g. Roland and McGuire 2009). However, the underlying mechanisms, which have initiated and driven this swarm, are not yet understood. Processes including temporary fluid overpressure, perhaps associated with creep might be drivers of the swarm, but the complex structure imaged by the relocated seismicity suggests that stress-transfer and sequential rupture of several small fault segments might play a role in the evolution of the sequence.
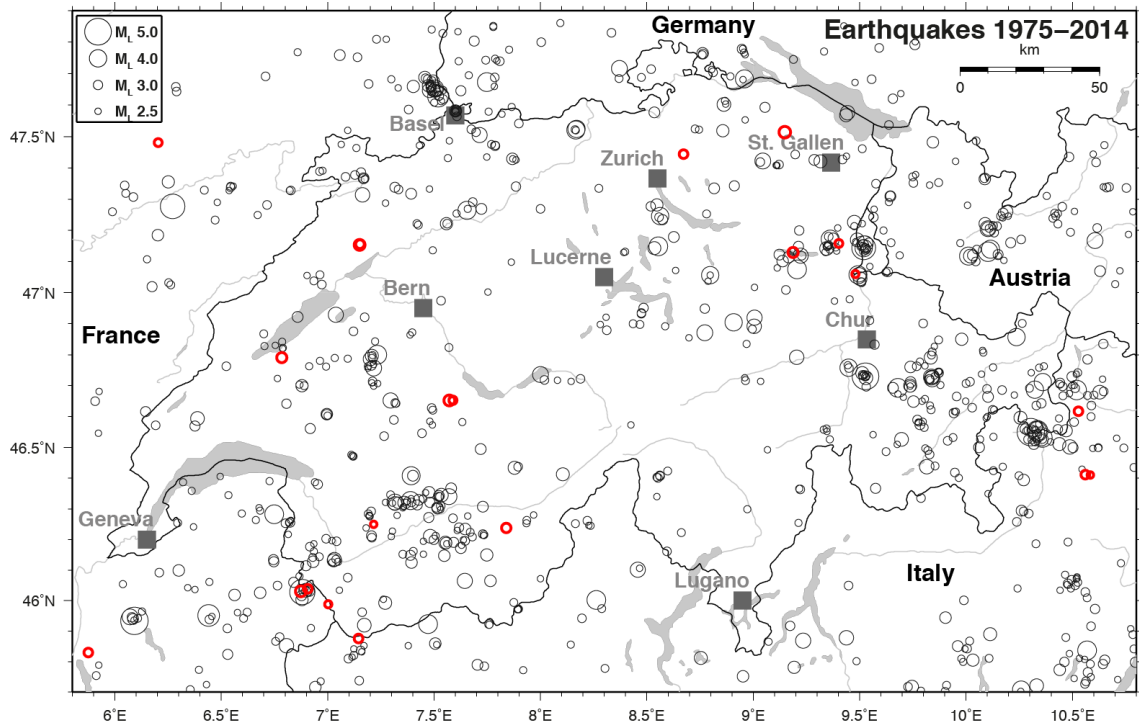
Figure 6 Epicentres of earthquakes with magnitudes $M_L \geq 2.5$, during the period 1975 – 2014. Grey circles denote earthquakes in the period 1975 – 2013, bold red circles indicate earthquakes in 2014.
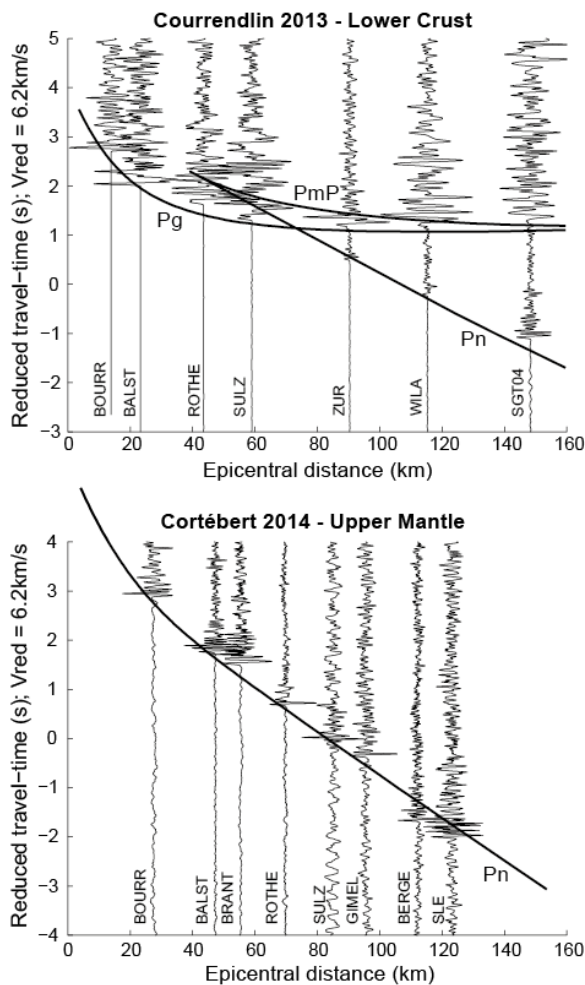

Figure 7 Record sections and travel-time curves for the Cortébert event of 2014 with a focal depth at 36 km in the upper mantle (lower panel) and the Courrendlin event of 2013 with a focal depth of 24 km in the lower crust (upper panel).

The ENE dipping structure highlighted by the sequence can neither be associated with known faults mapped at the surface nor with other instrumentally located seismicity prior to April 2014. However, the estimated epicentre of the historic Mw 5.2 Frutigen earthquake of 1729 is located only about 4 km to the SE of the sequence (Fäh et al. 2003). Considering the significant uncertainties in the location of historic events, it is possible that the fault that ruptured during the 1729 Mw 5.2 event is related to the fault system, which was active during the Diemtigen sequence.

3.2.6 Effretikon (ZH)

On November 8th, an M_L 2.8 earthquake occurred close to the village of Effretikon in the canton of Zürich (Fig. 2). The earthquake was felt in the region and triggered about 75 felt reports submitted to the SED website. The focal depth of the event is about 12 km, and therefore – as the events of the Frauenfeld sequence, about 20 km to the East – located in the crystalline basement below the Plateau Molasse. In contrast to the strongest event of the Frauenfeld sequence, the focal mechanism of the Effretikon earthquake is predominately strike-slip with an almost E-W oriented T-axis (Fig. 4, Table 3), typical for mid to lower crustal earthquakes in this region (e.g. Kastrup et al. 2004). The mechanisms of the Frauenfeld and Effretikon events reinforce the tendency of the azimuth of extensional T-axes to be oriented parallel to the strike of the Alpine orogen. Well-aligned T-axes, with a moderate plunge, are a predominant feature of the crust in the northern Alpine foreland (Deichmann 1990; Deichmann et al. 2000b; Kastrup et al. 2004; Singer et al. 2014).
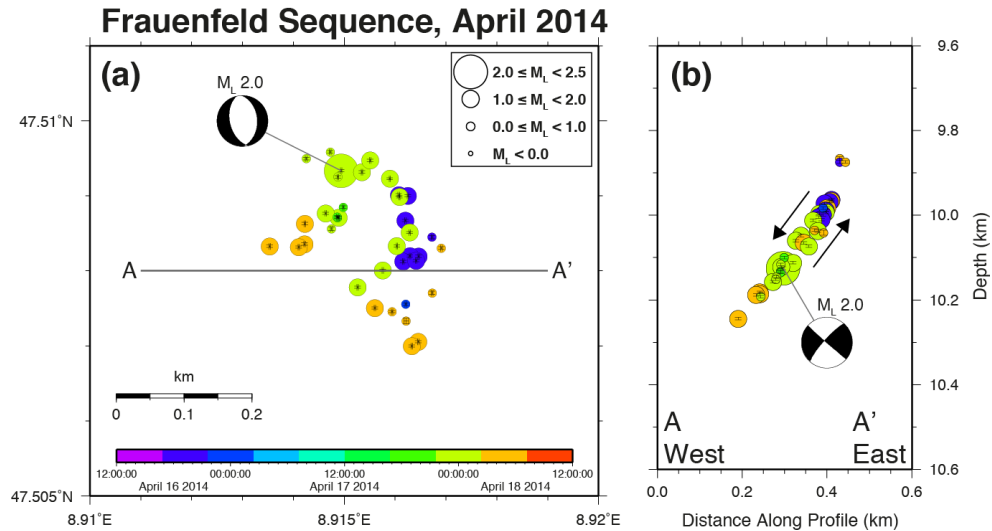
10

Figure 8 Relative relocations of the 3-day Frauenfeld sequence in April 2014 using double-difference techniques in combination with waveform cross-correlation: **a** map view; **b** vertical cross-section along an EW profile. Colors indicate origin time of the events. The focal mechanism of the M_L 2.0 event of April 17th is shown as lower hemisphere projection in map view and projected to the depth profile in cross-section.
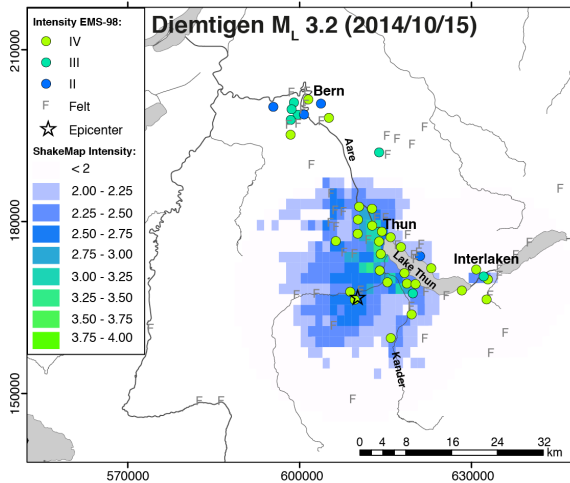

Figure 9 ShakeMap with intensities converted from instrumentally recorded ground motions of the M_L 3.2 Diemtigen event of October 15th. Colored dots mark macroseismic intensities (EMS-98) assessed by the SED based on about 430 felt reports submitted via the SED website. The star indicates the event epicentre. The felt intensities tend to indicate higher intensity levels than the instrumental ShakeMap close to the epicenter and in the urban areas of Bern and Interlaken.

3.2.7 Walensee (SG)

An interesting earthquake of M_L 3.1 occurred at the northern shore of the Walensee in eastern Switzerland (Fig. 2) on November 14th at 04:14 UTC. With a depth of 0 km, the event appears to have a very shallow source with a location a few hundred meters south of a closed quarry, which is situated about 2 km W of the village of Quinten. A sequence of ten earthquakes with M_L between 1.4 and 3.8 occurred 1-2 km below and within about 0.5 km horizontally from the same quarry in 1997. Deichmann et al. (1998) speculated that these events may have been triggered by activity at the nearby mine. Fig. 12 shows a comparison of the 2014 event with the three strongest events in 1997 recorded at

stations WIL and WILA. The distance between the two stations is less than 100 meters and can be neglected for this comparison. The similarity between the 2014 and the 1997 waveforms suggest that the 2014 event is part of the same cluster, with a similar location and focal mechanisms as the events in 1997 (Fig. 12). The distribution of available first motion polarities does not allow a well-constrained determination of the focal mechanism. Strike-slip as well as thrust mechanisms with N-S oriented P-axes fit the observed polarities equally well.
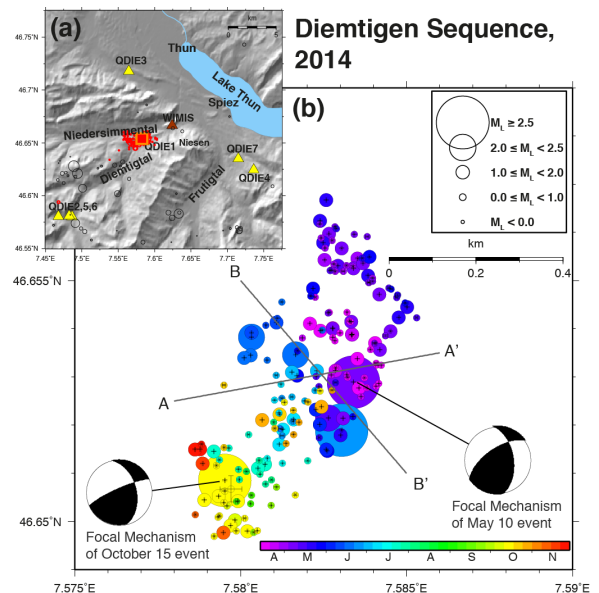

Figure 10 The Diemtigen sequence of 2014: **a** overview map with SED routine locations (red dots indicate earthquakes in 2014) and local seismic stations (brown triangle: SDSNet station WIMIS; Yellow triangles: temporary stations deployed by the SED). Orange box marks area shown in Fig. 10b; **b** relative relocations of a subset of 187 events of the sequence solving the double-difference equations by singular-value decomposition (SVD). Colors indicate origin time of the events. Crosses indicate relative location errors of epicentres.
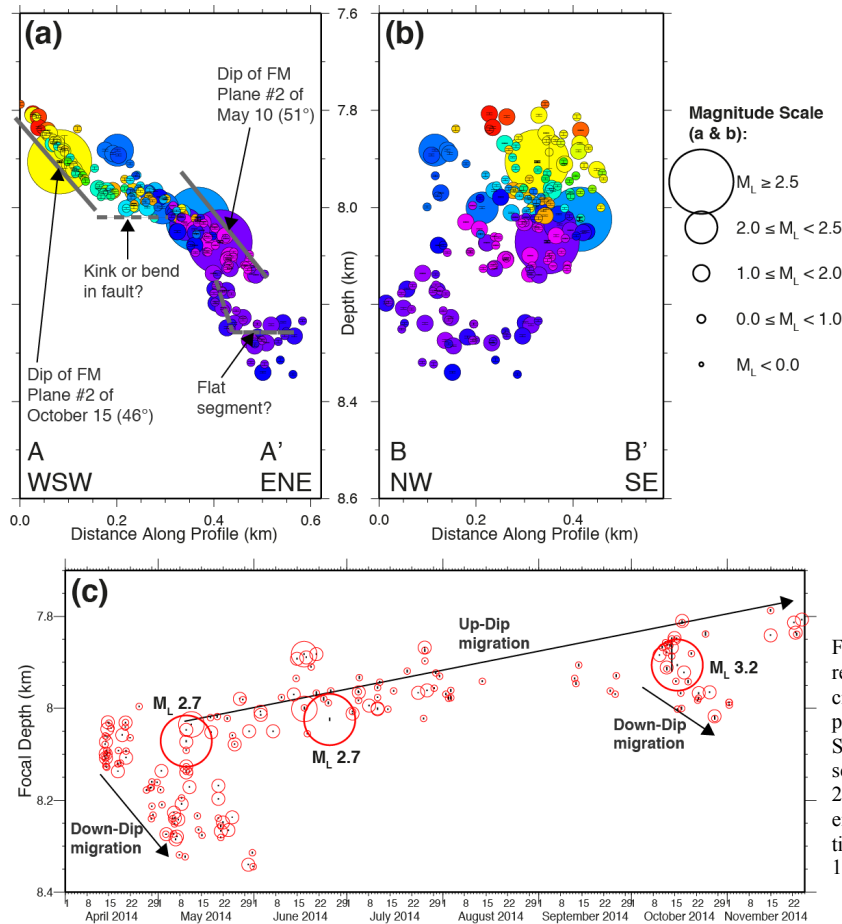
11

Figure 11 Depths distribution of relative relocations shown in Fig. 10. **a** vertical cross-section along a WSW-ENE striking profile; **b** vertical cross-section along a NW-SE striking profile; **c** vertical migration of seismicity between April and mid November 2014. Vertical bars indicate relative location errors of focal depths and colours indicate time evolution following colourbar of Fig. 10.

3.2.8 Vallorcine (France)

With 270 felt reports, the M_L 3.2 earthquake that occurred close to the village of Vallorcine (France) (Fig. 2) on November 23rd, was the second-most strongly felt earthquake in 2014. This earthquake is part of the on-going earthquake sequence that followed the M_L 4.9 earthquake of September 2005 (Deichmann et al. 2006; Fréchet et al. 2010; Diehl et al. 2013). Together with an M_L 3.2 event in December 2010, the M_L 3.2 of November 2014 is the second largest earthquake in the sequence since the mainshock of 2005. As in previous years, the region of Vallorcine was one of the seismically most active regions in 2014.

3.2.9 Werdenberg (SG)

An M_L 2.7 earthquake was located about 5 km E of Buchs (SG) in eastern Switzerland on December 7th (Fig. 2). The event is situated about 3 km SE of the Wildhaus sequence of 2009 (Deichmann et al. 2010; Marschall et al. 2013). The routinely determined focal depth of 4 km is well constrained by P and S-wave arrivals recorded at three strong-motion stations with epicentral distances from 3 to 6 km. The shallow focal depth suggests that the source is most likely located in the sediments, similar to the Wildhaus

earthquakes in 2009 (Deichmann et al. 2010; Marschall et al. 2013). The derived focal mechanism is strike-slip with a normal-fault component (Fig. 4), with orientations of P- and T-axes similar to the mechanisms in 2009.

3.2.10 Lower Crustal Earthquakes of Bürglen (TG) and Cheyres (FR)

The strongest earthquake in 2014 was the M_L 3.3 earthquake near Bürglen (TG) on December 15th (Fig. 2). With a focal depth of about 25 km it is located in the lower European crust. It was felt only sporadically (about 20 felt reports). The focal mechanism of this event is strike-slip with orientations of T- and P- axes typical for lower crustal earthquakes in northern Switzerland (Fig. 4). The M_L 3.1 Cheyres (FR) earthquake of December 17th, which is located close to the SW corner of Lake Neuchâtel (Fig. 2), is another example of a lower crustal earthquake. The Moho in this area is at about 31 km depth and the focal depth of 29 km indicates that the earthquake occurred just a few kilometers above the Moho. The predominately strike-slip mechanism shown in Fig. 4 is consistent with other lower crustal earthquakes in the region (Kastrup et al. 2004, Singer et al. 2014).
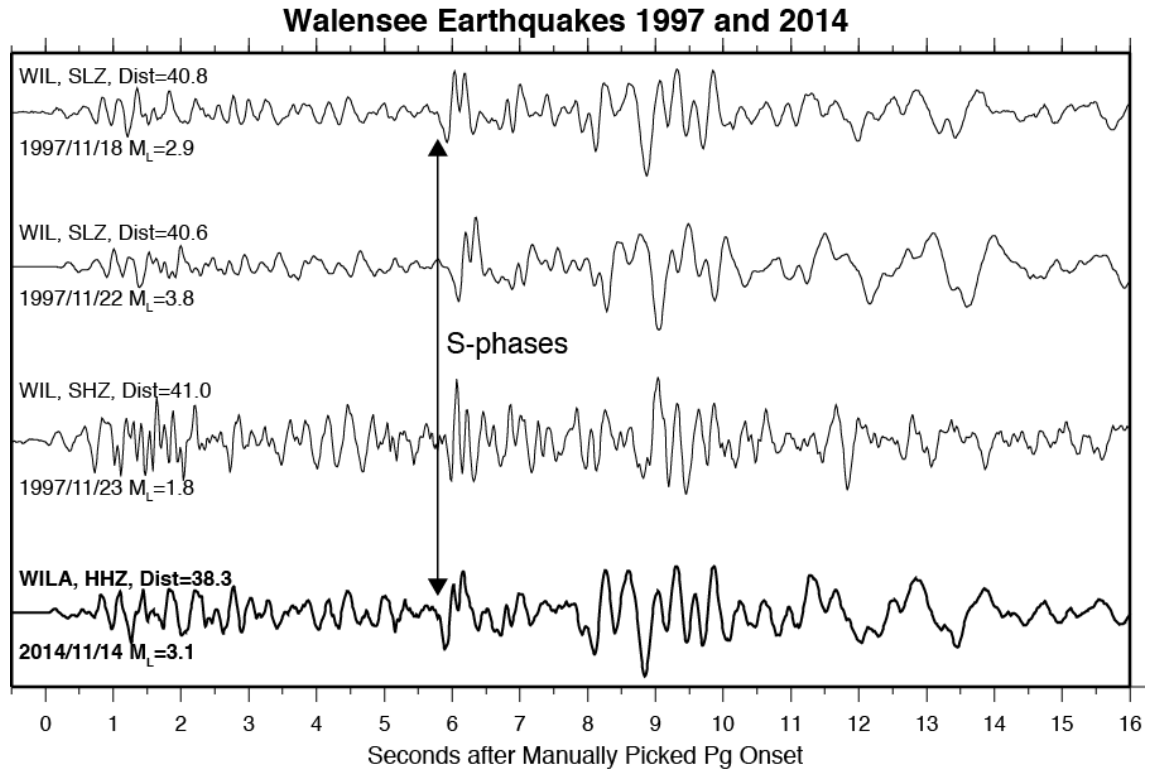
12

Figure 12 Comparison of vertical velocity seismograms of the M_L 3.1 Walenstadt event of November 14th 2014 recorded at station WILA (bottom trace, bold) and the Walenstadt sequence of November 1997 recorded at station WIL (top three traces).

3.2.11 Seismicity associated with the former Deep Heat Mining project in Basel

Over the time period 2008-2011, the seismic activity induced by the geothermal project in Basel in 2006 and 2007 (e.g. Deichmann and Giardini 2009) remained below the current automatic detection threshold of the SED (approx. M_L 0.9). In 2012 and 2013, the activity picked up again with seven detected events with magnitudes between M_L 0.9 and 1.8 (Diehl et al. 2014). For almost a whole year thereafter, activity, if at all, remained below the detection threshold until the occurrence of an M_L 1.6 event on December 23rd, 2014. With the exception of the M_L 1.1 event of October 3rd 2012, which was located about 500 m ESE and 400 m below the casing shoe, and thus clearly detached from all other events, the hypocenters of all the events recorded in 2012 and 2013 were located above the casing shoe at the SSE periphery of the previously stimulated rock volume (Deichmann et al. 2014). The hypocenter of the event of 2014, on the other hand, is located in a part of the stimulated rock volume that had already been activated in December 2006 and January 2007. A subsequent cross-correlation based analysis (for details on method see section 2.3) at borehole station MATTE (epicentral distance ~4 km) detected 9 additional events with magnitudes between $M_L^{(corr)}$ -0.4 and $M_L^{(corr)}$ 0.6 in December 2014. Four of these events had very similar waveforms to those of the

event of December 23rd, 2014, and were, therefore, located close to this event.

Using the same cross-correlation based detection as for 2014, we searched for additional undetected events in previous years. In the period from May 2012 to end of 2014, we found a total of 32 events in addition to the 9 events detected by the SED monitoring system. The magnitudes of these additional events range between $M_L^{(corr)}$ -0.6 and $M_L^{(corr)}$ 0.8. Whereas the large majority of these events can be associated with three clusters located at the periphery of the previously stimulated rock volume, two small events (M_L around 0), which occurred in February 2013, must be located close to the cluster that was active in December 2014. Thus it seems that the apparent migration of the seismicity back into the previously activated rock volume closer to the borehole observed at the end of 2014 started with some weak precursors already in the previous year. It has to be emphasized that the adopted set of template signals only covers four small, separate parts of the previously seismically active rock volume, and that the cross-correlation detection is therefore insensitive to events that might have occurred in other parts of this volume. Whether such events occurred is currently under investigation.

13

4. Discussion and Conclusion

In 2014, as in previous years, a large portion of the seismic activity was concentrated in the Valais, Graubünden, and their immediately adjacent regions (Fig. 2). Routinely calculated focal depths for all but 32 events recorded in 2014 are less than 16 km. Except for the Cortébert earthquake, all the deeper hypocenters occurred in the crust below the Molasse Basin and the Jura of northern Switzerland and southern Germany, with the main activity clustering between 7°E and 10°E (e.g. Deichmann et al. 2000a, Singer et al. 2014). The Cortébert event of January 2014, however, is the first documented earthquake with a hypocenter in the upper mantle in the northern Alpine foreland of Switzerland. Though the magnitude is only M_L 1.4, it shows that, contrary to common belief, the upper mantle in this region is not entirely aseismic. The Cortébert mantle event occurred 21 days after the M_L 2.8 and M_L 3.2 Biel earthquakes; its epicenter is located only about 2 km W of the Biel sequence. Given the relatively small magnitudes of the Biel events in combination with a vertical distance of about 30 km, a connection between the Biel and the Cortébert earthquakes appears very unlikely despite the noticeable proximity of epicenter and origin time.

Seismicity in 2014 was largely dominated by the occurrence of several earthquake sequences. On-going activity in the regions of Vallorcine and Balzers is related to the M_L 4.9 and M_L 4.1 earthquakes of the year 2005 and 2013, respectively. The sequences of Diemtigen and Frauenfeld, on the other hand, show the typical characteristics of earthquake swarms. High-precision hypocenter relocation in combination with available focal mechanisms identified a westward dipping normal fault in the crystalline basement in the Frauenfeld case. Seismogenic structures imaged in the Diemtigen sequence show ENE dipping structures associated with mechanisms composed of thrust and sinistral strike-slip components. The underlying mechanisms initiating and driving such earthquake swarms are not yet understood. The SED has therefore formed a working group to investigate these issues in more detail.

Although the maximum magnitude in 2014 reached only M_L 3.3, the unusually large number of 817 earthquakes was detected and located by routine analysis of the national seismic network over the year (Fig 3a). An additional 160 earthquakes with $M_L \leq 1.0$ have been located by supplementary analysis described in section 2.3. The total of 977 earthquakes is the largest number of events located within a year since the first installation of a seismic network in Switzerland in 1975. Between the year 2002 (completion of the SDSNet) and 2013, the average number of events recorded per year was about 540 (grey horizontal line in Fig. 3a). Compared to the average of previous years, the number of earthquakes (977) appears to have increased by more than 50% in 2014. As illustrated in Fig. 3a, this increase was mainly caused by the combination of two phenomena: **1)** The exceptionally vigorous earthquake sequences of Frauenfeld and Diemtigen contributed more than 200 events (Fig. 3a). **2)** On-going efforts to lower the thresholds for earthquake detection in Switzerland starting to have a significant impact on the total number of recorded events. Supplementary detection algorithms, on-going densification of the weak and strong-motion networks, as well as the deployment of temporary local networks (such as in the Diemtigen region) has improved the detection thresholds in certain parts of Switzerland. Excluding events of the two earthquake sequences and events located by supplementary earthquake analysis results in 607 earthquakes in 2014, a number close to the average of previous years. In summary it should be noted that the occurrence of two exceptional earthquake sequences and the on-going lowering of detection thresholds mainly explain the unusually large number of earthquakes in 2014. The total number of 22 earthquakes with $M_L \geq 2.5$, on the other hand, closely matches the yearly average of 23.0 events over the previous 39 years in this magnitude range. The total number of located earthquakes does therefore not allow conclusions on the overall seismic hazard in Switzerland.

References

Cauzzi, C., Edwards, B., Fäh, D., Clinton, J., Wiemer, S., Kästli, P., Cua, G., & Giardini, D. (2014). New predictive equations and site amplification estimates for the next-generation Swiss ShakeMaps. *Geophys. J. Int., 200*, 421–438. doi:10.1093/gji/ggu404.

Clinton, J., C. Cauzzi, D. Fäh, C. Michel, P. Zweifel, M. Olivieri, G. Cua, F. Haslinger and D. Giardini. (2011) The Current State of Strong Motion Monitoring in Switzerland, *in Earthquake Data in Engineering Seismology: Predictive Models, Data Management and Networks (Geotechnical, Geological and Earthquake Engineering),* Editors Akkar, S., Gülkan, P., and van Eck, T., ISBN 10: 9400701519 | 2011

Deichmann, N. (1990). Seismizität der Nordschweiz, 1987-1989, und Auswertung der Erdbebenserien von Günsberg, Läufelfingen und Zeglingen. *Nagra Technischer Bericht, NTB 90-46,* Nagra, Baden.

Deichmann, N., Baer, M., Ballarin Dolfin, D., Fäh, D., Flück, P., Kastrup, U., Kradolfer, U., Künzle, W., Mayer-Rosa, D., Röthlisberger, S., Schler, T., Sellami, S., Smit, P., Giardini, D. (1998). Earthquakes in Switzerland and surrounding regions during 1997. *Eclogae Geologicae Helvetiae 91(2),* 237-246.

Deichmann, N., Baer, M., Braunmiller, J., Ballarin Dolfin, D., Bay, F., Delouis, B., Fäh, D., Giardini, D., Kastrup, U., Kind, F., Kradolfer, U., Künzle, W., Röthlisberger, S., Schler, T., Salichon, J., Sellami, S., Spühler, E., Wiemer, S. (2000a). Earthquakes in Switzerland and surrounding regions during 1999. *Eclogae Geologicae Helvetiae, 93(3),* 395-406.

Deichmann, N., Ballarin Dolfin, D., Kastrup, U. (2000b). Seismizität der Nord- und Zentralschweiz. *Nagra Technischer Bericht, NTB 00-05,* Nagra, Wettingen.

Deichmann, N., Baer, M., Braunmiller, J., Husen, S., Fäh, D., Giardini, D., Kästli, P., Kradolfer, U., Wiemer, S. (2006). Earthquakes in Switzerland and surrounding regions during 2005. *Eclogae Geologicae Helvetiae - Swiss Journal of Geosciences, 99(3),* 443-452, DOI:10.1007/s00015-006-1201-1.

Deichmann, N. & Giardini, D. (2009). Earthquakes induced by the stimulation of an enhanced geothermal system below Basel (Switzerland). *Seismological Research Letters 80(5),* 784-798, doi:10.1785/gssrl.80.5.784.

Deichmann, N., Clinton, J., Husen, S., Edwards, B., Haslinger, F., Fäh, D., Giardini, D., Kästli, P., Kradolfer, U., Marschall, I., Wiemer, S. (2010). Earthquakes in Switzerland and surrounding regions during 2009. *Swiss Journal of Geosciences, 103(3),* 535-549, DOI:10.1007/s00015-010-0039-8.

Deichmann, N., Kraft, T., Evans, K. F. (2014). Identification of faults activated during the stimulation of the Basel geothermal project from cluster analysis and fault mechanisms for the larger magnitude events. *Geothermics, 52,* 84-97, DOI:10.1016/j.geothermics.2014.04.001.

Diehl, T., Deichmann, N., Clinton, J., Husen, S., Kraft, T., Plenkers, K., Edwards, B., Cauzzi, C., Michel, C., Kästli, P., Wiemer, S., Haslinger, F., Fäh, D., Kradolfer, U., Woessner, J. (2013). Earthquakes in Switzerland and surrounding regions during 2012. *Swiss Journal of Geosciences, 106,* 543-558, DOI:10.1007/s00015-013-0154-4.

Diehl, T., Clinton, J., Kraft, T., Husen, S., Plenkers, K., Guilhelm, A., Behr, Y., Cauzzi, C., Kaestli, P., Haslinger, F., Faeh, D., Michel, C., Wiemer, S. (2014). Earthquakes in Switzerland and surrounding regions during 2013. *Swiss Journal of Geosciences, 107,* 359-375, DOI:10.1007/s00015-014-0171-y.

Edwards, B., Allmann, B., Fäh, D., & Clinton, J. (2010). Automatic computation of moment magnitudes for small earthquakes and the scaling of local to moment magnitude. *Geophysical Journal International, 183(1),* 407-420, DOI: 10.1111/j.1365-246X.2010.04743.x.

Edwards, B., Kraft, T., Cauzzi, C., Kastli, P., & Wiemer, S. (2015). Seismic monitoring and analysis of deep geothermal projects in St Gallen and Basel, Switzerland. *Geophysical Journal International, 201,* 1020–1037. doi:10.1093/gji/ggv059.

Faenza, L. & Michelini, A (2010). Regression analysis of MCS intensity and ground motion parameters in Italy and its application in ShakeMap. *Geophys. J. Int., 180,* 1138–1152. doi: 10.1111/j.1365-246X.2009.04467.x.

Fäh, D., Giardini, D., Bay, F., Bernardi, F., Braunmiller, J., Deichmann, N., Furrer, M., Gantner, L., Gisler, M., Isenegger, D., Jimenez, M.-J., Kästli, P., Koglin, R., Masciadri, V., Rutz, M., Scheidegger, C., Schibler, R., Schorlemmer, D., Schwarz-Zanetti, G., Steimen, S., Sellami, S., Wiemer, S., & Wössner, J. (2003). Earthquake catalogue of Switzerland (ECOS) and the related macroseismic database. *Eclogae Geologicae Helvetiae - Swiss Journal of Geosciences, 96(2),* 219-236.

Fréchet, J., Thouvenot, F., Frogneux, M., Deichmann, N., & Cara, M. (2010). The M_w 4.5 Vallorcine (French Alps) earthquake of 8 September 2005 and its complex aftershock sequence. *Journal of Seismology, 15,* 43-58, DOI:10.1007/s10950-010-9205-8.

Grünthal, G. (1998). European Macroseismic Scale 1998 (EMS-98). Cahiers du Centre Européen de Géodynamique et de Séismologie 15, Centre Européen de Géodynamique et de Séismologie, Luxembourg, 99 pp.

Hardebeck, J.L., Shearer P.M. (2002). A new method for determining first-motion focal mechanisms. *Bulletin of the Seismological Society of America, 92,* 2264-2276.

Husen, S., Kissling, E., Deichmann, N., Wiemer, S., Giardini, D., Baer, M. (2003). Probabilistic earthquake location in complex three-dimensional velocity models: Application to Switzerland. *Journal of Geophysical Research, 108(B2),* 2077-2096.

Husen, S., E. Kissling, & von Deschwanden, A. (2012), Induced seismicity during the construction of the Gotthard Base Tunnel, Switzerland: hypocenter locations and source dimensions, *J. Seismol., 16(2),* 195-213, doi:10.1007/s10950-011-9261-8.

Kastrup, U., Zoback M.-L., Deichmann, N., Evans, K., Giardini, D., Michael, A.J. (2004). Stress field variations in the Swiss Alps and the northern Alpine foreland derived from inversion of fault plane solutions. *Journal of Geophysical Research, 109(B1),* doi:10.1029/2003JB002550B01402.

Lomax, A., Virieux J., Volant P., Thierry-Berge, C. (2000). Probabilistic earthquake location in 3D and layered models. In C.H. Thurber and N. Rabinowitz (Eds.), *Advances in Seismic Event Location,* (101-134), London: Kluwer Academic Publishers.

Marschall, I., Deichmann, N., Marone, F. (2013). Earthquake focal mechanisms and stress orientations in the eastern Swiss Alps. *Swiss Journal of Geosciences, 106,* 79-90, DOI:10.1007/s00015-013-0129-5.

Michel, C., Edwards, B., Poggi, V., Burjanek, J., Roten, D., Cauzzi, C., Fäh, D. (2014). Assessment of site effects in Alpine regions through systematic site characterization of seismic stations. *Bulletin of the Seismological Society of America, 104,* 2809-2826, doi: 10.1785/0120140097.

Nanjo, K.Z., D. Schorlemmer, J. Woessner, S. Wiemer, and D. Giardini (2010), Earthquake detection capability of the Swiss Seismic Network, *Geophysical Journal International, 181,* 1713-1724, doi:10.1111/j.1365-246X.2010.04593.x

Pfiffner, O. A., Sahli, S., & Stäuble, M. (1997a). Structure and evolution of the external basement massifs (Aar, Aiguilles-Rouges/Mt. Blanc). In O. A. Pfiffner, et al. (Eds.), Deep structure of the Alps, results of NRP20 (pp. 139–153). Basel: Birkhäuser.

Pfiffner, O. A., Erard, P.-F., & Stäuble, M. (1997b). Two cross sections through the Swiss Molasse Basin (lines E4-E6, W1, W7-W10). In O. A. Pfiffner, et al. (Eds.), Deep structure of the Alps, results of NRP20 (pp. 64–72). Basel: Birkhäuser.

Roland, E., & McGuire, J. J. (2009). Earthquake swarms on transform faults, *Geophys. J. Int., 178,* 1677-1690, doi:10.1111/j.1365-246X.2009.04214.x.

Schaff, D. P. & Waldhauser, F. (2010). One magnitude unit reduction in detection threshold by cross correlation applied to Parkfield (California) and China seismicity, *Bulletin of the Seismological Society of America, 100,* 3224–3238.

Singer, J., Diehl, T. Husen, S., Kissling, E. and Duretz, T. (2014), Alpine lithosphere slab rollback causing lower crustal seismicity in northern foreland, *Earth and Planetary*

Science Letters, *397*, 42-56, doi:10.1016/J.Epsl.2014.04.002.

Stange, S., Kurrle, D., Dahm, T., Hinzen, K.-G., Lehmann, K., Ritter, J.R.R., Schmidt, B. (2014), Subkrustale Seismizität in der Osteifel. Vortrag bei der 74. Jahrestagung der Deutschen Geophysikalischen Gesellschaft in Karlsruhe, 10.-13.3.2014.

Wagner, M., Kissling, E. and Husen, S. (2012), Combining controlled-source seismology and local earthquake tomography to derive a 3-D crustal model of the western Alpine region. *Geophysical Journal International, 191*, 789–802. doi: 10.1111/j.1365-246X.2012.05655.x.

Wald, D.J., Quitoriano, V., Heaton, T.H., Kanamori, H., Scrivner, C.W., & Worden, C.B. (1999). TriNet "ShakeMaps": Rapid generation of peak ground motion and intensity maps for earthquakes in southern California. *Earthquake Spectra, 15,* 537-555. doi: 10.1193/1.1586057

Waldhauser, F., Kissling, E., Ansorge, J., & Mueller, S. (1998), Three-dimensional interface modelling with two-dimensional seismic data: the Alpine crust-mantle boundary, *Geophys. J. Int., 135*(1), 264-278, doi:10.1046/j.1365-246X.1998.00647.x.

Waldhauser, F., & Ellsworth, W. L. (2000). A double-difference earthquake location algorithm: Method and application to the northern Hayward fault, California, *Bulletin of the Seismological Society of America, 90(6)*, 1353-1368, doi:10.1785/0120000006.

Worden, C. B., Wald, D. J., Allen, T. I., Lin, K., Garcia, D., & Cua G. (2010). A Revised Ground-Motion and Intensity Interpolation Scheme for ShakeMap, *Bulletin of the Seismological Society of America*, *100*, 3083-3096, doi:10.1785/0120100101.

Appendix 1 List of SED stations with online data acquisition that were operational at the end of 2014 (see Fig. 1).

National on-line network recorded in Zürich		
Code	Station name	Type
ACB	Acheberg, AG	BB
AIGLE	Aigle, VD	BB
BALST	Balsthal, SO	BB
BERGE	Lenzkirch, DE	BB
BERNI	Bernina, GR	BB
BNALP	Bannalpsee, NW	BB, SM
BOBI	Böbikon, AG (SP @ 154)	SP, SM
BOURR	Bourrignon, JU	BB, SM
BRANT	Les Verrières, NE	BB
DAGMA	Lutertal, Dagmarsellen, LU	BB
DAVOX	Davos, GR	BB
DIX	Grande Dixence, VS	BB, SM
EMBD	Embd, VS	BB
EMMET	Emmethof, AG	BB
EMING	Emmingen, DE	BB
EWZT2	Wetzwil, ZH	SP
FIESA	Fiescheralp, VS	BB
FLACH	Flach, ZH	EB
FUORN	Ofenpass, GR	BB
FUSIO	Fusio, TI	BB, SM
GIMEL	Gimel, VD	BB
GRIMS	Grimsel, BE	BB, SM
GRYON	Gryon, VS	EB
HAMIK	Hämikon, Dälikerfeld, LU (SP @ 140)	SP, SM
HASLI	Hasliberg, BE	BB
LAUCH	Lauchernalp, VS	BB
LIENZ	Kamor, SG	BB, SM
LKBD	Leukerbad, VS	EB
LKBD2	Leukerbad, VS	SP
LLS	Linth-Limmern, GL	BB, SM
METMA	Metma, DE	BB
MMK	Mattmark, VS	BB, SM
MUGIO	Muggio, TI	BB
MUO	Muotathal, SZ	BB
NALPS	Val Nalps, GR	BB
PANIX	Pigniu, GR	BB
PLONS	Mels, SG	BB
ROTHE	Rothenfluh, BL	BB
SALAN	Lac de Salanfe, VS	EB
SENIN	Senin, VS	BB, SM
SIMPL	Simplonpass, VS	BB
SLE	Schleitheim, SH	BB
STEIN	Stein am Rhein, SH	EB
STIEG	Oberembrach-Stiegenhof, ZH (SP @ 123)	SP, SM
SULZ	Cheisacher, AG	BB, SM
TORNY	Torny, FR	BB
TRULL	Trullikon, ZH	EB
VANNI	Vissoie, VS	BB
VDL	Valle di Lei, GR	BB, SM
WALHA	Wallhausen, DE	BB
WEIN	Weingarten, TG	EB
WILA	Wil, SG	BB
WIMIS	Wimmis, BE	BB
ZUR	Zürich-Degenried, ZH	BB, SM

Table A-1 High-gain seismograph stations of the Swiss national network operational at the end of 2014. Instrument type (all three-component): SP = 1-second, EB = 5-seconds, BB = broad-band, SM = accelerometer. The numbers in parentheses next to the borehole stations are the sensor depth with respect to ground surface in meters. Signals of LKBD2 are transmitted via analog telemetry.

On-line strong-motion network		
Code	Station name	Type
BIBA	Brigerbad, VS	SM
OTTER	Otterbach, BS	SM
SAIG	Aigle-Rue de la Gare, VD	SM
SALTS	Altdorf-Spital, UR	SM
SARE	Arbon, Evangelische Kirche, TG	SM
SARK	Sarnen-Kantonsschule, OW	SM
SAUR	Augst-Römermuseum, AG	SM
SBAF	Basel-Friedhofgasse, BS	SM
SBAK	Basel Klybeck, BS	SM
SBAJ2	Basel, St. Johann, BS	SM
SBAM2	Basel Münster, BS	SM
SBAP	Basel-PUK, BS	SM
SBAS	Baar, Spital, ZG	SM
SBAT	Basel-Tropenhaus, BS	SM
SBAV	Basel, Vogelsang, BS	SM
SBAW	Basel, Wirtschaftsgym., BS	SM
SBEG	Bettingen-Gewerbehaus, BS	SM
SBERN	Bern, kleine Schanze, BE	SM
SBIF2	Birsfelden, Friedhof, BL	SM
SBIK	Biel, Kongresshaus, BE	SM
SBIS2	Binningen, BS	SM
SBRS	Brig-Spital, VS	SM
SBUA2	Buchs Kindergarten, SG	SM
SBUB	Buchserberg Malbun, SG	SM
SBUH	Buchs, Hochschule, SG	SM
SCEL	Celerina, GR	SM
SCHS	Schaffhausen Spital, SH	SM
SCOU	Cournillens, FR	SM
SCUC	Scuol-Clozza, GR	SM
SCUG	Chur Gewerbeschule, GR	SM
SEMOS	Emosson Barrage, Bunker, VS	SM
SEPFL	Lausanne EPFL, VD	SM
SFRA	Frenkendorf, BL	SM
SGEV	Genf Feuerwehr, GE	SM
SGRA	Grächen-Ausblick, VS	SM
SIEB	Sierre-Ecole de Borzuat, VS	SM
SINS	Interlaken-Schloss, BE	SM
SIOM	Sion-Mayennets, VS	SM
SIOO	Sion-Ophtalmologie, VS	SM
SIOV	Sion-Valere, VS	SM
SKAF	Kaiseraugst-Friedhof, AG	SM
SLOP	Locarno, Pompieri, TI	SM
SLTM2	Linthal Matt, GL	SM
SLUB	Luzern Bramberg, LU	SM
SLUK	Luzern, Kirche, LU	SM
SLUW	Luzern Werkhofstr., LU	SM
SMAO	Martigny-Rue d'Octodure, VS	SM
SMFL	Mauren, Feuerwehr, FL	SM
SMUK	Muraz-Kläranlage, VS	SM
SMUR	Muraz-Reservoir, VS	SM
SMZW	Muttenz-Waldhaus, BL	SM
SNIB	Sankt Niklaus, VS	SM
SNES2	Neuenburg, Observatorium, NE	SM
SOLB	Solothurn Schule Bruhl, SO	SM
SOLZ	Solothurn-Zeughausgasse, SO	SM
SRER	Reinach Rainenweg, BL	SM
SRHB	Riehen-Bäumlihof, BS	SM
SRHE	Riehen, Erlensträsschen, BS	SM
SRHH	Riehen, Zur Hoffung, BS	SM
SSCN	Schweizerhalle, Novartis, BL	SM
STAF	Tafers, FR	SM
STGK	St. Gallen-Kloster, SG	SM
STRW	Triesenberg, Werkhof, FL	SM
STSP	Tschierv, GR	SM
SVAM	Vaz-Muldain, GR	SM
SVIL	Visp-Litternaring, VS	SM
SVIO	Visp-Obere Stapfeng., VS	SM
SVIT	Visp-Terbinerstr., VS	SM
SYVP	Yverdon Rue du Phil, VD	SM
SZER	Zernez, GR	SM
SZUZ	Zürich, Zeughauswiese, ZH	SM

Table A-2 Strong-motion stations of the Swiss national network with on-line data acquisition operational at the end of 2014. Instrument type (all three-component): SM = accelerometer.

Code	Station name	Type
Basel borehole network		
MATTE	Schüzenmatte (553)	SP (4.5Hz)
OTER1	Otterbach (500)	BB, SM
OTER2	Otterbach (2740)	SP (4.5Hz)
St. Gallen network		
SGT00	Sennhüslen (SP @ 205)	SP (4.5Hz), SM
SGT01	Gaiserwald	BB
SGT02	Zihlschlacht	BB
SGT03	Degersheim	BB
SGT04	Schlatt-Haslen	BB
SGT05	Eggersriet	BB
Rock Physics Lab monitoring networks		
MTI01	Mont Terri, ME Nische, JU	SM
MTI02	Mont Terri, HE Schacht, JU	BB
MTI03	Mont Terri, Brunefarine, St-Ursanne, JU	SM
GSF01	Oberhasli, Gelmersee, BE	SP

Table A-3 Local seismic networks with on-line data acquisition operational at the end of 2014. Instrument type (all three-component): SP = 1-second, unless otherwise indicated, BB = broad-band, SM = accelerometer. The numbers in parentheses next to the borehole stations are the sensor depth with respect to ground surface in meters.